

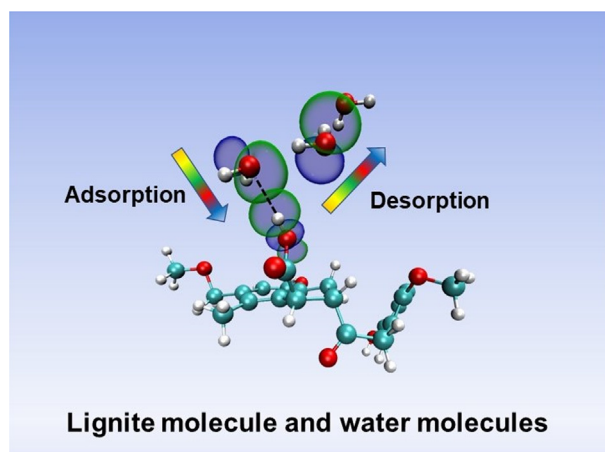


Full Length Article

Car-Parrinello molecular dynamics study on the interaction between lignite and water molecules

Zhengyang Gao^a, Chuanzhi Ma^{a,*}, Gang Lv^{b,*}, Ang Li^a, Xiang Li^a, Xiaoshuo Liu^a, Weijie Yang^a^a School of Energy and Power Engineering, North China Electric Power University, Baoding 071003, China^b School of Mathematics and Physics, North China Electric Power University, Baoding 071003, China

GRAPHICAL ABSTRACT



ARTICLE INFO

Keywords:

Lignite
Water adsorption
DFT
CPMD
Water reorientation

ABSTRACT

Water-desorption from lignite surface is an important issue in energy usage, however, corresponding researches are inadequate. Herein, in order to comprehensive understand the process of water-desorption from lignite surface, the interaction between water molecules and carboxyl group of lignite were investigated systematically from 298.15 K to 440 K, by using Car–Parrinello molecular dynamics (CPMD) method. The result indicated that in the key carboxyl group, the hydrogen site (H51) showed stronger adsorption capacity for water molecules than the oxygen site (O23) of the carboxyl group. Based on the statistical result, the water molecules adsorbed at H51 and O23 were considered as removed after 360 K. Vibration analysis was performed to acquire stretching frequencies of carboxyl group before and after water adsorption. The NBO analysis was used to study the re-orientation of water molecules in a 0.14 ps trajectory when they replace with each other. The NBO orbitals obtained show that when water molecule is replacing, the two lone pair orbitals of O31 and O32 interact with the σ antibonding orbital of O24–H51 bond at the same time. It enhances the formation of new H-bond and facilitates the fracture of old H-bond. This work can not only reveal the mechanism of water desorption from lignite, but also lay valuable foundations for efficient utilization of lignite resource.

* Corresponding authors.

E-mail addresses: mazhi19950907@163.com (C. Ma), glv7@ncepu.edu.cn (G. Lv).<https://doi.org/10.1016/j.fuel.2019.116189>

Received 2 June 2019; Received in revised form 6 September 2019; Accepted 7 September 2019

Available online 11 September 2019

0016-2361/ © 2019 Elsevier Ltd. All rights reserved.

1. Introduction

Coal has been widely considered to be one of the main efficient fossil resources for hundreds years in human society, due to its considerable reserves, high calorific value, and relative low cost [1]. Currently, even though application of new energy emerges and develops quickly, the role of coal resource played in conventional industry still can hardly be substituted in recent decades.

Coal-fired power plants are recognized as the largest consumer of coal resource. Among plenty of coals burned in coal-fired power plants, lignite was the most popular, because of its compelling advantages involving abundant reserves [2–4], low mining cost, high volatile matter, and trace content of hazardous elements [5,6]. However, there are still obvious obstacles for lignite usage in actual operation due to its high water content [7], which may well bring about energy waste of latent heat, potential spontaneous combustion hazard [8], increasing cost of transportation and storage, and promotion effect on CO₂ releasing [9–12]. In detail, considering previous studies, as high as 20–25% of the heat generated by lignite combustion was wasted to remove the associated water in fuel [13,14]. Therefore it is necessary to take measures to decrease the water content of lignite to a suitable level (about 5–10%) [15]. In other words, lignite must be upgraded before utilized [16,17].

The species and form of water in lignite is a key issue of moisture desorption, because the desorption temperature of water is directly involved with its species. Therefore large amounts of researches, both in experiment and in theory, have explored it deeply. Based on the previous experiments [11,18–22], and in the light of experiment data of differential scanning calorimetry and proton magnetic resonance methods depending on congelation characteristics, Norinaga et al. identified the water into free water, bound water and nonfreezable water [23]. Li et al. classified the water in coal into two categories through diffuse reflectance FTIR (DRIFT) experiments: (1) free water and water combined the coal surface with weak H-bonds; (2) water which is tightly H-bonded with coal surface [24]. Theoretically, Arisoy et al. classified the water as three kinds: bonded water, adsorbed water and free water, which were held by chemical bond, physiochemical forces and physicommechanical forces, respectively, by numerical simulation [8].

The type and quantity of functional groups on the surface of coal have a great influence on its chemical properties. First, these groups exhibit strong hydrophilicity [11,25–27], which allow the pore surface of lignite to absorb a large amount of water. Therefore, lignite has a high moisture content. As these groups are removed, the lignite gradually loses its hydrophilicity [28]. Xin et al. used lignite microwave dehydration technology and proved that the oxygen-containing functional groups is one of the most important factors affecting the interface stability of dehydrated lignite [29]. Wang et al. showed that the oxygen-containing functional groups play an important role in the water adsorption process by chemical titration method [30]. By using the electrostatic potential (ESP) analysis, Liu et al. indicated that the hydrophilic surface and high moisture content of lignite are attributed to the presence of oxygen-containing functional groups [31]. Therefore, the influence of oxygen-containing functional groups in coal is crucial to the adsorption of water on coal.

Xin et al. obtained the content distribution of functional group in lignite based on the in situ Fourier infrared spectrometry and the results indicated the order of its functional group content: methyl group > hydroxyl group > carboxyl group [32]. Both of the studies by Svarbova and Suuberg et al. have shown that the carboxyl and hydroxyl groups of lignite have an important role in the adsorption of water [33,34]. Gao et al. compared the water adsorption capacity of different functional groups in lignite by Density Functional Theory (DFT) simulation, and the result suggested that the carboxyl group in lignite is the strongest site [35]. Nishino et al. compared the carboxyl group with other oxygen-containing functional groups, and the results

demonstrated that the carboxyl group was the major part of the adsorption by FTIR and ionic thermal current adsorption experiments for water vapor. They did not find that the adsorption of water molecules was related to hydroxyl groups, although the concentration of hydroxyl groups is greater than carboxyl groups [36]. Liu and Zhang et al. obtained the order of hydrophilicity of the oxygen-containing functional groups of lignite as follows: carboxyl group > hydroxyl group > methyl group [37,38]. From the above studies, it could be seen that the carboxyl group was the strongest functional group of lignite to adsorb water, and its content was relatively high. Therefore, the carboxyl groups play a vital role in the hydrophilicity of lignite.

In addition, the effects of temperature on lignite dehydration were researched in practical engineering applications. Through diffuse reflectance FTIR experiments, Li et al. concluded that the free water and adsorbed water connected to lignite via weak H-bond would be removed when the temperature was lower than 80 °C, while the water connected to lignite through strong H-bond would be removed when the temperature was above 80 °C [24]. Miura et al. used the in-situ diffuse reflectance IR Fourier transform (DRIFT) technique and concluded that the produced water was mainly contribute to the desorption of adsorbed water or the decomposition of COOH groups, i.e., the pyrolysis reaction when the temperature is below 140 °C or above 140 °C, respectively. In other words, the moisture of the coal is completely removed at 140 °C [39].

It is noticed that the above experimental studies did not clarify the details of the interaction between lignite and water molecule and the dehydration mechanism of them at the molecular level. Meanwhile, the corresponding DFT calculation did not take into account the effects of actual conditions, such as temperature. It is known that the classical molecular dynamics (MD) simulations could be effective to account for conditions involving temperature, pressure, and solvents with atomistic resolution [40]. Furthermore, the Car-Parrinello molecular dynamics (CPMD) allows researchers to use density functional theory to provide a better quantum mechanical description for system evolution by introducing the fictitious electronic kinetic energy term into the Lagrangian. Researchers have used it to explore the structural and properties of water system or water related systems [41,42]. Therefore, in order to explore the effect of temperature on the adsorption of water on lignite molecule, we model a realistic interaction between water and lignite in gas phase environment by CPMD method. It aids the interpretation of experimental data and providing new insight.

2. Methods

In this paper, the lignite molecular model proposed by Kumagai et al was used, who demonstrated that this model can represent the characteristics of lignite when it removes water [43]. The lignite model is shown in Fig. 1, which contains hydroxyl, carboxyl, carbonyl, methoxyl, two benzene rings and one pentabasic cycle. For the complex of

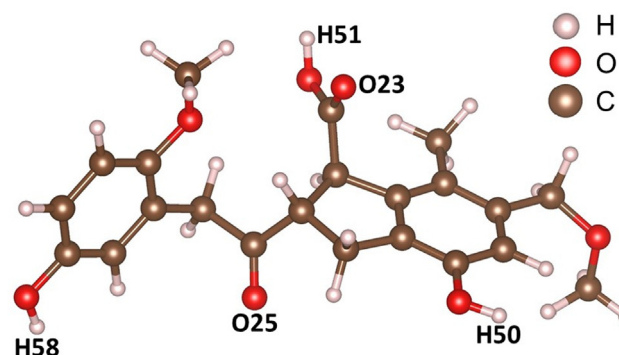


Fig. 1. The structure of lignite molecule and the atomic number of the selected atoms.

lignite and water, we used the initial configuration of randomly placing twelve water molecules near the carboxyl group for research according to the previous studies [35,44,45].

The Car-Parrinello molecular dynamics method [46] was used to study the system of lignite and water molecules in gas phase environment. All calculations were performed by DFT calculation with Perdew-Burke-Ernzerhof (PBE) [47] exchange-correlation functional and Vanderbilt (VDB) pseudopotentials. Periodic boundary conditions were imposed using cubic supercells with the box size of $20 \times 14 \times 16 \text{ \AA}^3$, which contains one lignite molecule and twelve water molecules. Kohn-Sham orbitals were expanded in plane waves up to a kinetic energy cutoff of 25.0 Ry. In the dynamical simulations, the fictitious electronic mass of 400.0 a.u. and a time step of 0.1 fs were used. We selected 298.15 K, 320 K to 440 K as the simulation temperature, in which the later increases from 320 K to 440 K by 20 K. The NVT ensemble and the Nosé-Hoover thermostat method were used and the simulation time is 30 ps.

The relevant ESP charge of the lignite molecule, and the change of vibration stretching frequency of carboxyl group, before and after the adsorption of water molecules were calculated to reveal the relation between water molecules and oxygen-containing functional groups. We also calculated the Natural Bond Orbitals (NBOs) [48] associated with the carboxyl group to explain the replacing interaction of water and lignite. The ESP charge and vibration stretching frequency were calculated by CPMD and the NBO analysis was carried out by Gaussian 09 [49]. The VMD [50] program was used for the molecular and orbital visualization.

3. Results and discussion

3.1. MD analysis

We simulated the interaction between lignite molecule and twelve water molecules, which in the vicinity of the carboxyl group in initial configuration. From the trajectory of dynamics, we did not find a significant interaction between water molecules and the benzene ring of lignite molecules, so the H-bond interaction between the carboxyl group and water molecules is considered to influence the dewater process. According to the van der Waals radius of the H atom (1.06 Å) and the O atom (1.42 Å) [51], considering the gas phase environment, we have uniformly selected 3.20 Å as the statistical distance of H-bonds at different temperatures.

Based on the dynamic trajectory, the statistics for the interacting time of water molecules formed H-bonds with H51 or O23 at different temperatures were made and their average values were shown in Fig. 2. The data of the interacting time and its dependence on temperature characterize the water adsorption capability of the two sites in the carboxyl group.

It can be clearly seen from the Fig. 2 that at the two sites of the carboxyl group, i.e., O23 and H51, the interacting time of water molecules has a significant decrease section as temperature increasing. The significant decrease occurs for O23 or H51 at 298.15–340 K or 298.15–360 K, respectively, indicating that the temperature in these two range has a significant impact on their adsorption capability. From the trend of the curves in Fig. 2 by statistical analysis, the turning point at 340 K or 360 K is responsible to distinguish the sharp downtrend and steady trend. The difference of interacting time for O23 or H51 showed that the adsorption capability for water molecules after 340 K or 360 K was significantly weaker than before.

As for the corresponding temperature at the beginning of smooth trend for the two curves, 360 K (H51) is higher than 340 K (O23). That is to say, H51 shows its weak ability to adsorb water molecules at a higher temperature than O23. In the meantime, the average interaction time of water molecules adsorption of H51 was stronger than that of O23 at each temperature. These results indicated that H51 exhibits a stronger adsorption capability for water molecules than O23. The water

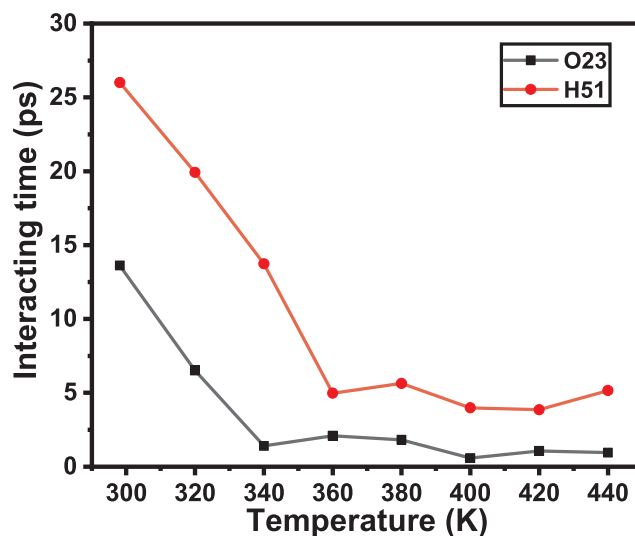


Fig. 2. Average interacting time of water molecules at O23 or H51 of the carboxyl group.

molecules adsorbed at H51 and O23 were considered as removed after 360 K from the aspect of interacting time. Proximately, the result is consistent with the experimental data of Li et al, i.e., the water molecules linked by weak H-bonds in lignite would be completely removed at 80 °C (353.15 K) in relevant experiment [24].

In order to better show the difference in the adsorption capability of water molecules between the O23 and H51 at 360 K in details, we selected one typical trajectory and the dependence of the distance between O23 or H51 and the water molecule on time is shown in Fig. 3. The H65 ~ H86 in (a) or O32 ~ O40 in (b) represent the H atoms or the O atoms that form H-bonds with O23 or with H51 in different water molecules, respectively. It can be seen that the adsorption and desorption of water molecules at O23 occur more frequently. For the H51, the adsorption and desorption phenomena occur only once within the same period of time. The frequency of desorption of water molecules at O23 or H51 is 0.48n/s or 0.2n/s, respectively, in which the former was 2.4 times more than the latter. Therefore, it can be clearly observed that the adsorption capability of H51 sites for water molecules was significantly stronger than that of O23 sites.

3.2. ESP charge and vibrational stretching frequency analysis

The ESP charge of the optimized lignite molecule were calculated and the results were shown in Fig. 4. The charge 0.48 e of H51 in the carboxyl group was higher than the charge of the H site of the other functional groups, and the charge -0.58 e of O23 was also higher than the charge of the O site of the other functional groups. It can be seen that the carboxyl group has stronger adsorption capability for water molecules than other functional groups in lignite molecule from the aspect of static electricity.

Based on the results of CPMD, the lignite molecule with two water molecules were selected to optimized. Then the vibrational stretching frequency of the O–H and C=O bond of the carboxyl group before and after adsorption of water were calculated and the corresponding results were shown in Table 1. It showed that before adsorption, the stretching frequency of O–H or C=O bond in carboxyl group was 3568.6 cm^{-1} or 1715 cm^{-1} , respectively. After adsorption, the stretching frequency of the O–H or C=O bond in carboxyl group was 3378.84 cm^{-1} or 1650.18 cm^{-1} , which was consistent with the relevant experimental results for carboxyl group [52,53]. It can be seen that the adsorption decreases the vibrational stretching frequencies of O–H and C=O bond by 189.76 cm^{-1} and 65.05 cm^{-1} , respectively. When no water molecules were adsorbed, the bond length of O–H and C=O bond in

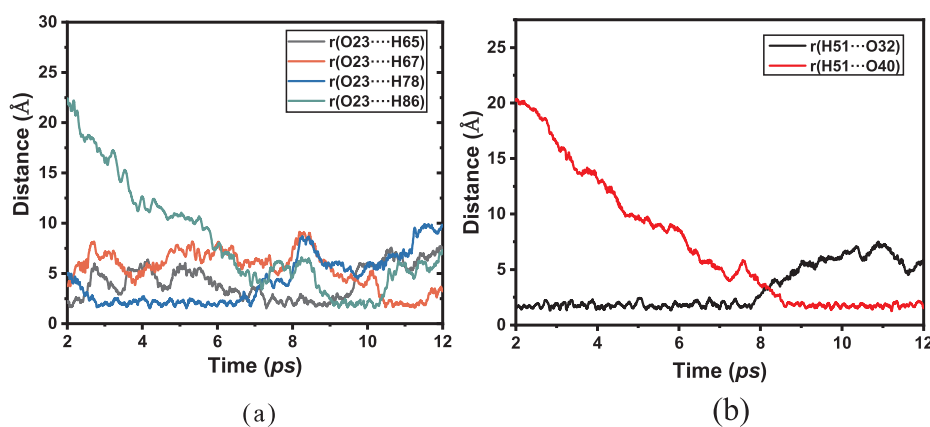


Fig. 3. The dependence of the distance between O23 (a) or H51 (b) in the carboxyl group and water molecule at 360 K on time.

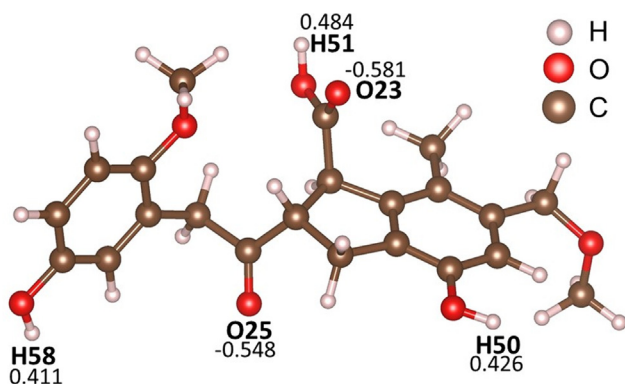


Fig. 4. The ESP charge (in a.u.) for the selected atoms of lignite molecule.

Table 1

The vibrational stretching frequency and bond length of C=O and O–H of carboxyl group after the adsorption of water molecules.

	f (Δf) (cm^{-1}) ^a	R (ΔR) (\AA) ^b
C=O	1650.18 (–65.05)	1.24(0.02)
O–H	3378.84 (–189.76)	1.01(0.03)

a f or Δf represents the vibrational stretching frequency or its change, respectively.

b R or ΔR represents the bond length or its change, respectively.

carboxyl group was 0.98 \AA and 1.22 \AA , respectively. After the water molecules were adsorbed, the bond length of the O–H and C=O bond increased to 1.01 \AA and 1.24 \AA , respectively. The adsorption increased the bond length of C=O and O–H bond by 0.03 \AA and 0.02 \AA , respectively. Combined with the change of the vibration frequency, the interaction caused the elongation of the O–H and C=O bond and brings the stretching frequency shifted towards the red corresponding, making these two bonds weaker.

3.3. Replacement phenomenon of the water

It is worth mentioning that the replacement phenomenon of water molecules, i.e., a new water molecule replaced the previous water molecule adsorbed, occurs at almost all the temperatures except 298.15 K, in which the water molecules exhibits quite stable adsorption with carboxyl group at this temperature. Meanwhile, at 320 K and 340 K, the replacement phenomenon occurs only at O23, but not at the strongest H51. When the temperature rises to 360 K, this phenomenon occurs at both of the two sites.

It is generally believed that the process of water molecules forming new H-bond is the breaking of old H-bond firstly, and then the

formation of new H-bond. But Damien et al. found, by using the molecule dynamics simulation for water system, that water molecules form new H-bonds is through the twisting action of the O–H bond, weakening the connection with the previous hydrogen donor and forming H-bond with the new hydrogen acceptor [54]. At this point, the old H-bond has not yet broken. After that, the O–H bond continues to twist, and the old H-bond disappears. In present simulation, the replacement or reorientation process is indeed observed, which is similar to the water reorientation.

In order to understand the mechanism of reorientation, we selected the trajectory at 380 K for analysis. The replacement occurs at H51 (H-bond donor) and the dependence of the relevant distance ($r_{\text{H51-O}}$) on time was shown in Fig. 5. The replacement starts from 6.4 ps, in which the O31 in 31th water molecule (W31) is close to the H51 in carboxyl group at this time. Then the H-bond between H51 with O31 is broken after ~ 1 ps, and the water molecule containing the O32 in 32th water molecule (W32) comes to acts with H51 and the reorientation begins.

To visually reveal this phenomenon, we selected three typical stages in the replacement process and plotted them in Fig. 6. The H51 of the carboxyl group first formed a H-bond with O31 in W31, and then the O24–H51 bond of the carboxyl group flips from O31 toward O32, as shown in Fig. 6(a). With the close of W32, the H51 of the carboxyl group simultaneously formed H-bond with the W31 and the W32, as shown in Fig. 6(b). As the torsion phenomenon continued, shown in Fig. 6(c), the H-bond between the H51 and the W31 was broken, and then the W31 left. Starting from 6.8 ps, a stable H-bond was formed

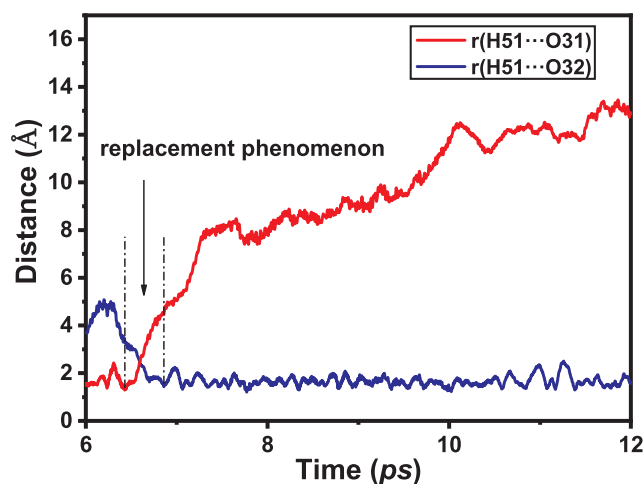


Fig. 5. The dependence of the distance between H51 in the carboxyl group and the corresponding oxygen atom in water molecule at 380 K on time, with the corresponding time interval of the replacement phenomenon marked.

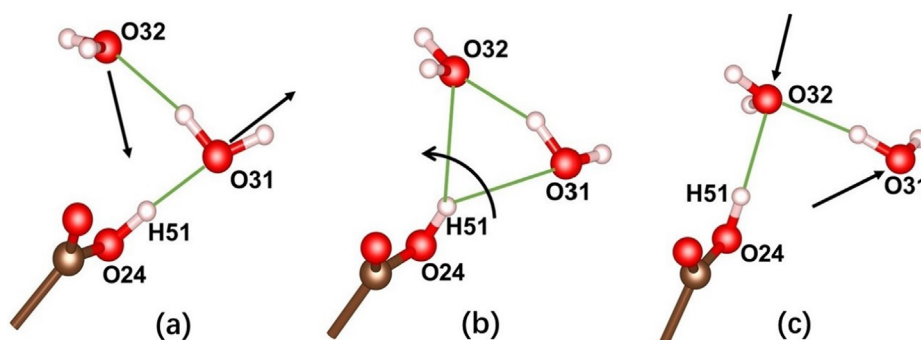


Fig. 6. Three typical stages in the H-bond exchange mechanism, in which the green lines represent the H-bond and the black arrows represent the key movements. (For interpretation of the references to colour in this figure legend, the reader is referred to the web version of this article.)

between the H51 of the carboxyl group and the O32 of W32. At this time, the reorientation completed and hence the replacement of water molecules was finished.

In order to explore the switching in geometry, we extract a total of 0.14 ps (6.53–6.67 ps, 70 frames in total) of trajectory around the timepoint, i.e., 6.6 ps in Fig. 5, for research. The R_{O24^*O31} , R_{O24^*O32} and θ were shown in Fig. 7(a) and their dependence on time were shown in Fig. 7(b). The angle θ represents the angle between the projection of the O24–H51 bond of the carboxyl group on the O31–O24–O32 plane and the angle bisector of the angle O31–O24–O32. This definition of θ allows it to be unaffected by the O24–H51 bond motion relative to the O31–O24–O32 plane and the change of the O31–O24–O32 angle. When θ equals 0, H51 is approximately equidistant from O31 and O32. Therefore, it can well reflect the torsion phenomenon of O24–H51 bond between O31 and O32. The fluctuation of θ at 6.62–6.66 ps was due to a slight swing of the O24–H51 bond of the carboxyl group, which is considered as the influence of thermal motion. These results are consistent with the reorientation result computed by Damien et al. [54].

In addition, we calculated the ESP charge of O31, O32 and H51 in the 0.14 ps trajectory to understand the interaction in view of electronic structure. The dependence of the ESP charge of the O31 and O32 in two water molecules and the H51 in the lignite on time were calculated and shown in Fig. 8. It can be seen that the charge of the oxygen atoms in water molecules and H51 in carboxyl group exhibits a negative and positive property, respectively.

We can notice that from 6.58 ps, with the approach of W32, the charge of the O32 increased obviously, hence increasing its attraction to the H51, and reducing the attraction between O31 and H51. At 6.60 ps, the distance between O31 or O32 and H51 is 2.46 Å or 2.49 Å, respectively, and the corresponding ESP charge of O32 and O31 was -1.02 and -0.98 e., respectively. Both of the distance or charge values are close to other one, respectively. After 6.60 ps, the distance between

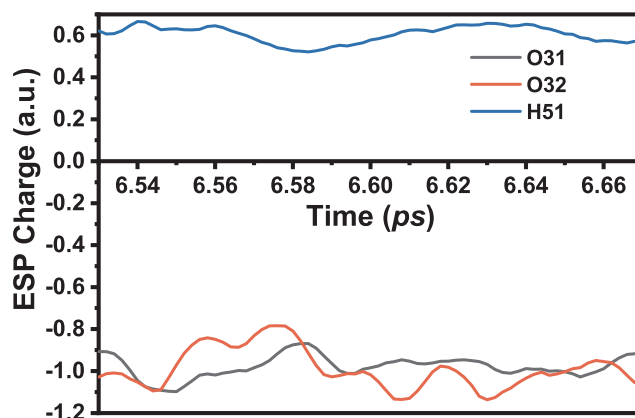


Fig. 8. The dependence of the ESP charge of O31, O32 and H51 on time.

O32 and H51 decreased, and therefore the ESP charge of O32 increased. Conversely, the distance between O31 and H51 increased, and in the meanwhile the ESP charge of O31 decreased. The change in ESP charge, increase or decrease, can be consistent with the approach of W32 and the departure of W31.

We selected the initial, middle and the end configuration of the replacement phenomenon (6.53 ps, 6.60 ps and 6.67 ps) in Fig. 5 to calculate the NBO orbitals and the corresponding results were shown in Fig. 9. As for the initial configuration of 6.53 ps in Fig. 9(a), the distance between H51 and O31 or O32 is 2.04 Å or 3.90 Å, respectively. According to the widely accepted H-bond criterion [55,56], the distance indicated there was a H-bond between H51 and W31, and the interaction between H51 and W32 is almost nonexistent. It is obvious that the σ antibonding orbital of O24–H51 bond is close to the lone pair orbital of O31, and is far from the one of O32. And the corresponding

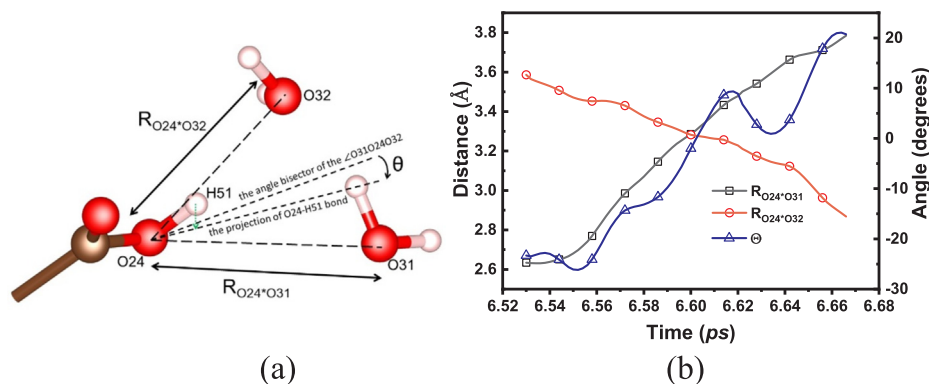


Fig. 7. (a) R_{O24^*O31} or R_{O24^*O32} represents the distance between O24 (carboxyl) and O31 (W31) or O32 (W32), respectively. (b) The dependence of R_{O24^*O31} , R_{O24^*O32} and θ on time of the corresponding trajectory.

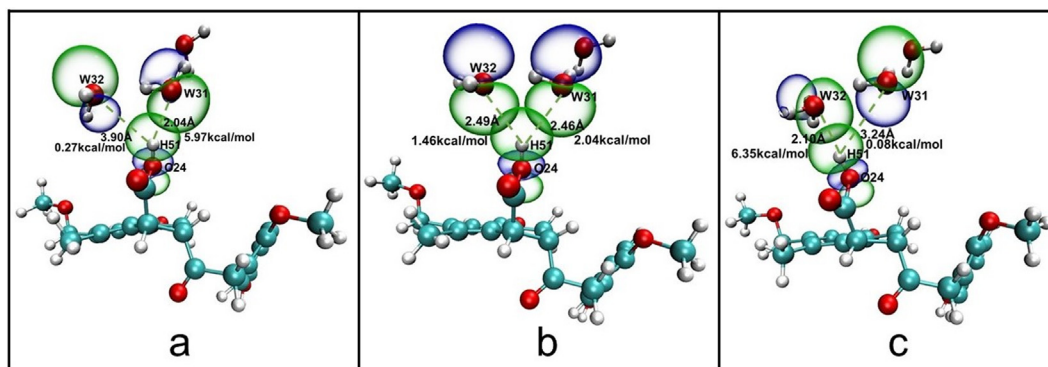


Fig. 9. The NBOs of three configurations at the initial, middle and the end of the replacement phenomenon.

second-order perturbation stabilization energies of them is 5.97 kcal/mol or 0.27 kcal/mol, respectively.

As for the middle configuration of 6.60 ps in Fig. 9(b), i.e., which is the timepoint of the replacement phenomena, the distance between H51 and O31 or O32 is 2.46 Å or 2.49 Å (approximately equidistant), respectively. Each lone pair orbital of O31 or O32 is close to the σ antibonding orbital of O24–H51 bond, in which the electrons of the two lone pair orbitals of O31 and O32 are simultaneously transferred to the σ antibonding orbital of O24–H51 bond. The corresponding second-order perturbation stabilization energies decreased to 2.04 kcal/mol and 1.46 kcal/mol, respectively. It indicated that when water molecule was replacing, the two lone pair orbitals of O31 or O32 would interact with the σ antibonding orbital of O24–H51 bond at the same time. This state makes the interaction between H51 and the two water molecules very weak. Furthermore, the inertia generated by the previous movement, i.e., the approach of W32 and the departure of W31, could strengthen the new H-bond between H51 and W32 and weaken the old H-bond between H51 and W31.

As for the end configuration of 6.60 ps in Fig. 9(c), i.e., the W31 left H51 and the W32 was adsorbed at H51, the distance between H51 and O31 increased to 3.24 Å. In contrast, the distance between H51 and O32 decreased to 2.10 Å. At this time, the σ antibonding orbital of O24–H51 is far away from the lone pair orbital of O31 and it interacts with the lone pair orbital of O32. The corresponding second-order stabilization energies are 0.08 kcal/mol and 6.35 kcal/mol, respectively. Finally, a stable H-bond is formed between W32 and H51, and the interaction between W31 and H51 is relatively weak.

4. Conclusion

To summary, we used the first principles and CP molecular dynamics to explore the interaction between lignite and water molecules and the dependence of interacting time on temperature. The results show that the adsorption capability of O23 or H51 in lignite for water molecules above 340 K or 360 K is significantly weaker than below 340 K or 360 K, respectively. The interacting time demonstrates that the adsorption of H51 of carboxyl group is stronger than O23. We calculated the charge of the lignite molecule and the vibrational stretching frequency before and after the carboxyl group interacting with water molecules. From the aspects of electronic properties, the obtained ESP charge proved that the adsorption capacity of carboxyl groups on water molecules is stronger than other functional groups. Furthermore, the reorientation of water molecules when they replace with each other was analyzed by NBO and dynamic charge analysis. The results show that when water molecule is replacing, the close distance between H51 and O23 or O24, the similar NBO orbitals and the close second-order stabilization energies of them indicate that the two lone pair orbitals of O31 or O32 interact with the σ antibonding orbital of O24–H51 bond at the same time. This simultaneous effect contributes to the occurrence of replacement, and would help to strengthen a new H-bond and

fracture an old H-bond.

Acknowledgement

This work was supported by the Beijing Municipal Natural Science Foundation (2182066), the Natural Science Foundation of Hebei Province of China (B2018502067) and the Fundamental Research Funds for the Central Universities under Grants (2017MS161, JB2015RCY03 and 2017XS121). This work was carried out at LvLiang Cloud Computing Center of China, and the calculations were performed on TianHe-2.

References

- [1] Yu J, Tahmasebi A, Han Y, Yin F, Li X. A review on water in low rank coals: the existence, interaction with coal structure and effects on coal utilization. *Fuel Process Technol* 2013;106:9–20.
- [2] Tahmasebi A, Yu J, Li X, Meesri C. Experimental study on microwave drying of Chinese and Indonesian low-rank coals. *Fuel Process Technol* 2011;92(10):1821–9.
- [3] Sakaguchi M, Laursen K, Nakagawa H, Miura K. Hydrothermal upgrading of Loy Yang Brown coal – effect of upgrading conditions on the characteristics of the products. *Fuel Process Technol* 2008;89(4):391–6.
- [4] Gao J-r, Tao X-x, Hou T, Wan Y. Progress of lignite drying and dehydration technology. *Clean Coal Technol* 2008;6:73–6.
- [5] Willson WG, Walsh DAN, Irwin W. Overview of low-rank coal (LRC) drying. *Coal Preparation* 1997;18(1–2):1–15.
- [6] Li X, Rathnam RK, Yu J, Wang Q, Wall T, Meesri C. Pyrolysis and combustion characteristics of an Indonesian low-rank coal under O₂/N₂ and O₂/CO₂ conditions†. *Energy Fuels* 2010;24(1):160–4.
- [7] Ohm T-I, Chae J-S, Lim J-H, Moon S-H. Evaluation of a hot oil immersion drying method for the upgrading of crushed low-rank coal. *J Mech Sci Technol* 2012;26(4):1299–303.
- [8] Arisoy A, Akgün F. Modelling of spontaneous combustion of coal with moisture content included. *Fuel* 1994;73(2):281–6.
- [9] Kabir KB, Hein K, Bhattacharya S. Process modelling of dimethyl ether production from Victorian brown coal—integrating coal drying, gasification and synthesis processes. *Comput Chem Eng* 2013;48:96–104.
- [10] Tahmasebi A, Yu J, Han Y, Zhao H, Bhattacharya S. Thermogravimetric study and modeling for the drying of a Chinese lignite. *Asia-Pac J Chem Eng* 2013;8(6):793–803.
- [11] Allardice D, Clemow L, Favas G, Jackson W, Marshall M, Sakurovs R. The characterisation of different forms of water in low rank coals and some hydrothermally dried products. *Fuel* 2003;82(6):661–7.
- [12] Domazetis G, Barilla P, James BD, Glaisher R. Treatments of low rank coals for improved power generation and reduction in Greenhouse gas emissions. *Fuel Process Technol* 2008;89(1):68–76.
- [13] Karthikeyan M, Kuma JVM, Hoe CS, Ngo DLY. Factors affecting quality of dried low-rank coals. *Drying Technol* 2007;25(10):1601–11.
- [14] Karthikeyan M, Zhonghua W, Mujumdar AS. Low-rank coal drying technologies—current status and new developments. *Drying Technol* 2009;27(3):403–15.
- [15] Jeon D, Kang T, Kim H, Lee S, Kim S. Investigation of drying characteristics of low rank coal of bubbling fluidization through experiment using lab scale. *Sci China Technol Sci* 2011;54(7):1680–3.
- [16] Gupta R. Advanced coal characterization: a review. *Energy Fuels* 2007;21(2):451–60.
- [17] Xu C, Xu G, Zhao S, Zhou L, Yang Y, Zhang D. An improved configuration of lignite pre-drying using a supplementary steam cycle in a lignite fired supercritical power plant. *Appl Energy* 2015;160:882–91.
- [18] Li C-Z. *Advances in the Science of Victorian Brown Coal*. Elsevier; 2004.
- [19] Lynch LJ, Webster DS. Effect of thermal treatment on the interaction of brown coal

- and water: a nuclear magnetic resonance study. *Fuel* 1982;61(3):271–5.
- [20] Mraw SC, O'Rourke D. Water in coal pores: the enthalpy of fusion reflects pore size distribution. *J Colloid Interface Sci* 1982;89(1):268–71.
- [21] Mraw S, Naas-O'Rourke D. Water in coal pores: low-temperature heat capacity behavior of the moisture in Wyodak coal. *Science* 1979;205(4409):901–2.
- [22] Vorres KS. Effect of temperature, sample size, and gas flow rate on drying on Beulah-Zap lignite and Wyodak subbituminous coal. *Energy Fuels* 1994;8(2):320–3.
- [23] Norinaga K, Kumagai H, Hayashi J-i, Chiba T. Classification of water sorbed in coal on the basis of congelation characteristics. *Energy Fuels* 1998;12(3):574–9.
- [24] Li D-T, Li W, Li B-Q. In situ diffuse reflectance FTIR study on water in lignite. *Chem J Chin Univ* 2002;23(12):2325–8.
- [25] Charriere D, Behra P. Water sorption on coals. *J Colloid Interface Sci* 2010;344(2):460–7.
- [26] Yu Y, Liu J, Wang R, Zhou J, Cen K. Effect of hydrothermal dewatering on the slurryability of brown coals. *Energy Convers Manage* 2012;57:8–12.
- [27] Chen P, Gu M, Chen X, Chen J. Study of the reaction mechanism of oxygen to heterogeneous reduction of NO by char. *Fuel* 2019;236:1213–25.
- [28] Ja Murray, Evans D. The brown-coal/water system: Part 3. Thermal dewatering of brown coal. *Fuel* 1972;51(4):290–6.
- [29] Xin FW, Xu ZQ, Tu YN, Yang W, Han XY, Geng PF. Dehydration and upgrading of lignite with microwave. *Appl Mech Mater* 2013;423–426:667–73.
- [30] Wang Y, Zhou J, Bai L, Chen Y, Zhang S, Lin X. Impacts of inherent O-containing functional groups on the surface properties of Shengli lignite. *Energy Fuels* 2014;28(2):862–7.
- [31] Liu J, Wu J, Zhu J, Wang Z, Zhou J, Cen K. Removal of oxygen functional groups in lignite by hydrothermal dewatering: an experimental and DFT study. *Fuel* 2016;178:85–92.
- [32] Xin H-H, Wang D-M, Qi X-Y, Xu T, Dou G-L, Zhong X-X. Distribution and quantum chemical analysis of lignite surface functional groups. *J. Univ. Sci. Technol. Beijing* 2013;35(2):135–9.
- [33] Švábová M, Weishauptová Z, Přibyl O. Water vapour adsorption on coal. *Fuel* 2011;90(5):1892–9.
- [34] Suuberg EM, Otake Y, Yun Y, Deevi SC. Role of moisture in coal structure and the effects of drying upon the accessibility of coal structure. *Energy Fuels* 1993;7(3):384–92.
- [35] Gao Z, Ding Y, Yang W, Han W. DFT study of water adsorption on lignite molecule surface. *J Mol Model* 2017;23(1):27.
- [36] Nishino J. Adsorption of water vapor and carbon dioxide at carboxylic functional groups on the surface of coal. *Fuel* 2001;80(5):757–64.
- [37] Liu J, Jiang X, Cao Y, Zhang C, Zhao G, Zhao M, et al. Exploring the effect of oxygen-containing functional groups on the water-holding capacity of lignite. *J Mol Model* 2018;24(6):130.
- [38] Zhang Y, Jing X, Jing K, Chang L, Bao W. Study on the pore structure and oxygen-containing functional groups devoting to the hydrophilic force of dewatered lignite. *Appl Surf Sci* 2015;324:90–8.
- [39] Miura K, Mae K, Li W, Kusakawa T, Morozumi F, Kumano A. Estimation of hydrogen bond distribution in coal through the analysis of OH stretching bands in diffuse reflectance infrared spectrum measured by in-situ technique. *Energy Fuels* 2001;15(3):599–610.
- [40] Tilocca A, Cormack AN. Modeling the water–bioglass interface by ab initio molecular dynamics simulations. *ACS Appl Mater Interfaces* 2009;1(6):1324–33.
- [41] Vandevondele J, Mohamed F, Krack M, Hutter Jr., Sprik M, Parrinello M. The influence of temperature and density functional models in ab initio molecular dynamics simulation of liquid water. *J Chem Phys* 2005;122(1):9080.
- [42] Silvestrelli PL, Bernasconi M, Parrinello M. Ab initio infrared spectrum of liquid water. *Chem Phys Lett* 1997;277(5–6):478–82.
- [43] Kumagai H, Hayashi J, Chiba T, Nakamura K. Change in physical and chemical characteristics of brown coal along with a progress of moisture release. *Fuel Energy Abstracts* 1999;43(10):2.
- [44] Xiao J, Zhao Y-P, Fan X, Cao J-P, Kang G-J, Zhao W, et al. Hydrogen bonding interactions between the organic oxygen/nitrogen monomers of lignite and water molecules: a DFT and AIM study. *Fuel Process Technol* 2017;168:58–64.
- [45] Tang H-Y, Wang X-H, Feng L, Cao Z-X, Liu X. Theoretical study on the interactions between the lignite monomer and water molecules. *Struct Matter Quantum Chem* 2015;89(9):1605–13. CJRJoPCA.
- [46] Hutter J, Alavi A, Deutch T, Bernasconi M, Goedecker S, Marx D, et al. CPMD; Copyright IBM Corp 1990-2008, Copyright MPI fur Festkörperforschung Stuttgart 1997-2001. nd.
- [47] Perdew JP, Burke K, Ernzerhof M. Generalized gradient approximation made simple. *Phys Rev Lett* 1996;77(18):3865.
- [48] Reed AE, Curtiss LA, Weinhold F. Intermolecular interactions from a natural bond orbital, donor-acceptor viewpoint. *Chem Rev* 1988;88(6):899–926.
- [49] Frisch M, Trucks G, Schlegel H, Scuseria G, Robb M, Cheeseman J, et al. *Gaussian 09, Revision D. 01, 2013, Gaussian. 2013.*
- [50] Humphrey W, Dalke A, Schulten K. VMD: visual molecular dynamics. *J Mol Graph* 1996;14(1):33–8.
- [51] van der Bondi A. Waals volumes and radii. *J Phys Chem* 1964;68(3):441–51.
- [52] Dioumaev AK, Braiman MS. Modeling vibrational spectra of amino acid side chains in proteins: the carbonyl stretch frequency of buried carboxylic residues. *J Am Chem Soc* 1995;117(42):10572–4.
- [53] Danecek P, Kapitan J, Baumruk V, Bednarova L, Kopecky Jr. V, Bour P. Anharmonic effects in IR, Raman, and Raman optical activity spectra of alanine and proline zwitterions. *J Chem Phys* 2007;126(22):224513.
- [54] Laage D, Hynes JT. A molecular jump mechanism of water reorientation. *Science* 2006;311(5762):832–5.
- [55] Kumar R, Schmidt J, Skinner J. Hydrogen bonding definitions and dynamics in liquid water. *J Chem Phys* 2007;126(20):05B611.
- [56] Wernet P, Nordlund D, Bergmann U, Cavalleri M, Odelius M, Ogasawara H, et al. The structure of the first coordination shell in liquid water. *Science* 2004;304(5673):995–9.